Proceedings of the 19th Lunar and Planetary Science Conference, pp. 147-161

High Alumina (HA) and Very High Potassium (VHK) Basalt Clasts from Apollo 14 Breccias, Part 2—Whole Rock Geochemistry: Further Evidence for Combined Assimilation and Fractional Crystallization Within the Lunar Crust

C. R. Neal and L. A. Taylor

Department of Geological Sciences, University of Tennessee, Knoxville, TN 37996-1410

R. A. Schmitt and S. S. Hughes

Radiation Center, Oregon State University, Corvallis, OR 97331

M. M. Lindstrom

Mail Code SN2, NASA Johnson Space Center, Houston, TX 77058

The understanding of basalt petrogenesis at the Apollo 14 site has increased markedly due to the study of "new" samples from breccia "pull-apart" efforts. Whole-rock compositions of 26 new high alumina (HA) and 7 very high potassium (VHK) basalts emphasize the importance of combined assimilation and fractional crystallization in a lunar regime. Previously formulated models for HA and VHK basalt petrogenesis are modified in order to accommodate these new data, although modeling parameters are essentially the same. The required range in HA basalt compositions is generated by the assimilation of KREEP by a "primitive" (high MG#, low SiO_2, low incompatible elements) parental magma. In order to generate all observed compositions, the inferred parental magma must undergo 70% fractional crystallization and 15.4% KREEP assimilation. The VHK basalts can be generated by three parental HA basalts (primitive, intermediate, and evolved) assimilating granite. In order to accommodate the compositional variability of granite, three granite assimilant compositions are used in the modeling. Results indicate that VHK basalt compositions are dominated by the parental magma, and only up to 8% granite assimilation is required. This modeling indicates that at least three VHK basalt flows must be present at the Apollo 14 site.

INTRODUCTION

The role of igneous processes in a lunar regime is becoming better understood as our database increases. The post magma ocean era is particularly important as it details the evolution and composition of the newly-formed lunar crust and mantle. This evolution may be observed in the study of extruded basaltic magmas (e.g., *Dickinson et al.*, 1985, 1988; *Shervais et al.*, 1985a,b; *Goodrich et al.*, 1986; *Neal et al.*, 1988a,b). There has also been an evolution of models developed to explain the range of basaltic compositions at the Apollo 14 site. Previously (*Shervais et al.*, 1985a; *Dickinson et al.*, 1985), it was envisaged that there existed groups of basalts, which were derived from different source regions. With the analysis of "new" basalt samples, *Neal et al.* (1988a,b) demonstrated the importance of combined assimilation and fractional crystallization in the petrogenesis of basalts at the Apollo 14 site. It was demonstrated that high alumina (HA, after the classification of *Irving*, 1975) and very high potassium (VHK) basalts can be generated by an interaction of a basaltic magma with KREEP and granite, respectively. Because some VHK basalts also contain a KREEP signature, the idea of a granite-KREEP association is reinforced (*Ryder*, 1976; *Neal and Taylor*, 1988).

As a continuation of our previous endeavors, we have studied new, pristine basaltic clasts in breccias from the Apollo 14 site (*Neal et al.*, 1988c,d,e), which include both HA and VHK basalt types. We use the term HA to describe a basalt containing between 11-14 wt.% Al_2O_3 and <0.3 wt.% K_2O, with K/La ratios of approximately 100. The term VHK is used to describe a basalt containing >0.3 wt.% K_2O, a K_2O/Na_2O ratio >1, and a K/La ratio >150. In addition, Rb and Ba may also be enriched relative to HA basalts. The major-element chemistry of VHK basalts is generally similar to HA basalts, except for elevated K_2O contents.

The present study involves the examination of the whole-rock chemistry from 26 new HA and 7 new VHK basalt clasts by instrumental neutron activation analysis (INAA). These clasts were extracted from breccias 14303, 14304, and 14321. This paper is part 2 of a two-part contribution, the first detailing the mineralogy and petrography of these basalts (*Neal et al.*, 1989). In the following presentation, samples are referred to by probe mount (PM) number first, with the INAA number following in brackets. This allows comparison with the mineralogy and petrography of these samples detailed in part 1. The aim of this paper is to include these new compositions in the models previously proposed for HA and VHK basalt petrogenesis (*Neal et al.*, 1988a,b). This should provide an adequate test of previous models formulated for basalt petrogenesis at the Apollo 14 site. With the extension of the basalt database, minor refinements to the preexisting models are likely to be necessary.

WHOLE-ROCK CHEMISTRY

The whole-rock chemistry for most of the samples was determined by INAA at Oregon State University by RAS and SSH, but four VHK basalts [14303,328(318); 14304,169(168); 14304,177(176); and 14304,203(180)] were determined by INAA at NASA Johnson Space Center (JSC) by MML. [For analytical techniques, see *Hughes et al.* (1988) and *Lindstrom et al.* (1989).] Major elements were also determined by INAA except for these four VHK basalts. For these basalts, a split of the sample used for INAA was fused and quenched to glass in a nitrogen atmosphere on a molybdenum strip. The glass produced was then analyzed by electron microprobe using a broad beam. Molybdenum was included in the analysis and subtracted from the total, and the resulting analyses was normalized to 100. The major elements obtained from INAA (Fe, Ca, Na, K) show good agreement with totals from the electron microprobe. For example, the INAA results for 14304,169(168) give 0.59 wt.% Na_2O, 0.91 wt.% K_2O, 10.2 wt.% CaO, and 10.4 wt.% FeO. The fused bead analysis gave abundances of 0.60 wt.%, 0.96 wt.%, 10.8 wt.%, and 10.6 wt.%, respectively, for these elements. Silica was determined by difference for samples analyzed by INAA; this value is approximate, as the errors inherent in the analysis of other major elements will be magnified. The siderophile trace elements, Ir and Au, were not detected in both the HA and VHK basalts, consistent with the pristine nature of our samples.

As reported in part 1 of this presentation (*Neal et al.*, 1989), the textures of the HA basalts are generally fine to medium grained (grains are generally 0.1-2 mm in the longest dimension). Therefore, for a fine-grained basalt, a small sample size can give a representative whole-rock analysis. A larger sample size is required in order to obtain a representative analysis of a coarse-grained basalt. All analyzed samples with weights less than ≈25 mg are fine grained. However, although 14321,1604(1549) weighed only 9.5 mg and is medium grained, the analysis presented in Table 1 does not deviate substantially from other analysis using larger sample weights. The analyses of VHK basalts were generally conducted on larger samples than for the HA basalts (up to 115 mg: Table 2). Therefore we assume that our INA analyses are representative of the basalt clast and are not radically affected by heterogeneous sampling. The analytical results, as well as sample weights, are presented in Tables 1 and 2.

HA Basalts

Major and rare earth elements. The 26 new 14321 HA basalts exhibit a range of MG# (Table 1) from 44.0 to 55.2, with CaO ranging from 8.80 wt.% to 12.1 wt.%. Silica, although calculated by difference, also shows significant variation from 42.8 wt.% to 49.4 wt.% SiO_2, whereas Al_2O_3 exhibits less variation from 11-14 wt.%. TiO_2 reaches a maximum of 3.25 wt.% in 14321,1595(1530), and Na_2O is <0.61 wt.% in all samples.

Major-element compositions are represented on a Ol-An-Qz pseudoternary "Walker diagram" (*Walker et al.*, 1972, 1973) in Fig. 1. The new basalts have similar major element compositions to basalts previously reported from the Apollo 14 site (e.g., *Shervais et al.*, 1985a; *Dickinson et al.*, 1985; *Neal et al.*, 1988a). As a result of this similarity, phase boundaries are drawn for an Fe/(Fe+Mg) ratio of 0.6, determined by *Neal et al.* (1988a). This ratio is used because it represents the composition of the parental magma at the time it encounters the Ol-Plag cotectic. The abundance of K_2O ranges from 0.04-0.36 wt.%. The greatest abundance of K_2O is in (,1542) (0.36 wt.%), but this cannot be classified as a VHK as K_2O/Na_2O and K/La ratios are too low (0.6 and 76.3, respectively). Generally, K increases with increasing La/Lu and Sm/Eu ratios.

Abundances of the REE are presented in Table 1, and the range in chondrite-normalized REE profiles is presented in Fig. 2a. Primitive REE profiles are those with a $(La/Lu)_N$ ratio <1 and REE abundances ≈10× chondrite. More evolved REE profiles are those with $(La/Lu)_N$ ratios >1 and La abundances up to 120× chondrite. As the La/Lu ratio increases, so does the depth of the negative Eu anomaly, with the most evolved patterns mirroring KREEP. Comparison of these REE profiles with previously reported Apollo 14 basalts (Fig. 2b) demonstrates a widening of HA basalt compositions at the Apollo 14 site.

Trace elements. The new 14321 HA basalts exhibit moderate variation in the compatible (Sc, Cr, Ni, Co, and V) large ion lithophile (LIL: K, Rb, Ba, Sr, and Cs) and high field strength (HFS: Zr, Hf, Ta, U, and Th) elements (Table 1). These ranges are similar to those previously reported (*Dickinson et al.*, 1985; *Shervais et al.*, 1985a; *Neal et al.*, 1988a), although the upper limit for HFS elements is extended by our new data. The Ni, Ba, Cs, and U analyses for most of the HA basalts exhibit uncertainties too large to be of any petrogenetic

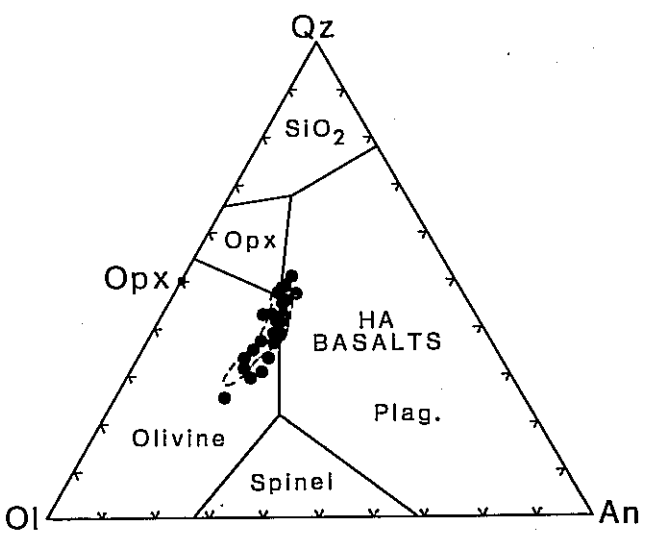

Fig. 1. Major element compositions of the HA basalts represented on an Ol-An-Qz pseudoternary (after *Walker et al.*, 1972, 1973). The dashed field represents previously reported HA basalts (*Dickinson et al.*, 1985; *Shervais et al.*, 1985a; *Neal et al.*, 1988a). Phase boundaries are drawn for Fe/(Fe+Mg) = 0.6 (see *Neal et al.*, 1988a).

TABLE 1. Whole rock compositions of 14321 HA basalts; values are in wt.% for oxides and in ppm for all other elements.

PM No.		,1482	,1483	,1484	,1485	,1601	,1591	,1592	,1593	,1594	,1595	,1596	,1597
INAA No.	,1445	,1448	,1449	,1451	,1454	,1518	,1520	,1522	,1524	,1529	,1530	,1533	,1535
Wt (mg)	23.3	49.9	57.7	36.7	45.4	15.7	24.8	30.1	52.7	23.3	20.7	28.5	55.3
SiO_2*	46.9	45.8	47.1	46.8	45.5	49.4	46.6	45.5	48.2	49.4	44.3	46.6	46.3
TiO_2	2.10 (11)	1.89 (13)	2.26 (14)	1.75 (11)	2.03 (13)	2.41 (11)	1.82 (10)	2.03 (12)	2.67 (17)	2.65 (12)	3.25 (13)	2.09 (11)	2.11 (13)
Al_2O_3	14.0 (2)	13.2 (2)	14.2 (2)	13.3 (2)	13.8 (2)	12.8 (12)	14.0 (2)	13.7 (2)	11.7 (2)	13.8 (2)	11.8 (1)	13.0 (2)	13.8 (2)
FeO	15.9 (1)	17.7 (1)	17.1 (1)	15.6 (1)	16.9 (1)	15.3 (1)	16.6 (1)	16.6 (2)	16.4 (1)	14.0 (1)	20.2 (1)	16.3 (1)	16.6 (1)
MnO	0.21 (1)	0.24 (1)	0.23 (1)	0.22 (6)	0.23 (1)	0.23 (1)	0.22 (1)	0.22 (1)	0.22 (1)	0.21 (1)	0.25 (1)	0.22 (1)	0.23 (1)
MgO	8.60 (50)	9.70 (60)	7.90 (60)	11.1 (4)	9.80 (60)	7.90 (50)	10.8 (5)	10.6 (5)	8.90 (60)	7.40 (60)	10.6 (5)	10.1 (4)	9.00 (60)
CaO	11.2 (5)	10.3 (5)	10.1 (5)	10.1 (5)	10.9 (6)	10.9 (50)	10.3 (5)	11.0 (5)	9.61 (53)	11.6 (5)	8.80 (40)	10.7 (5)	10.9 (5)
Na_2O	0.52 (1)	0.51 (1)	0.59 (1)	0.46 (1)	0.30 (1)	0.54 (1)	0.58 (1)	0.60 (1)	0.40 (1)	0.51 (1)	0.22 (1)	0.47 (1)	0.55 (1)
K_2O	0.17 (2)	0.14 (2)	0.16 (2)	0.13 (2)	0.06 (1)	0.16 (2)	0.19 (2)	0.18 (2)	0.07 (1)	0.16 (2)	0.04 (1)	0.11 (1)	0.13 (2)
Sc	55.3 (1)	59.0 (1)	61.5 (1)	55.7 (1)	60.7 (1)	54.3 (1)	51.4 (1)	56.2 (1)	60.8 (1)	51.6 (1)	45.0 (1)	56.4 (1)	58.2 (1)
V	104 (5)	118 (5)	119 (6)	143 (6)	142 (6)	104 (5)	99 (5)	122 (5)	129 (6)	100 (5)	125 (5)	119 (5)	112 (5)
Cr	3420 (10)	3840 (10)	2690 (10)	4690 (10)	4670 (10)	2790 (10)	2890 (10)	3480 (10)	4230 (10)	2540 (10)	4650 (10)	3330 (10)	3330 (10)
Co	34.2 (1)	34.9 (1)	26.2 (1)	29.9 (1)	38.2 (1)	34.1 (1)	33.0 (1)	33.7 (1)	39.5 (1)	35.4 (1)	44.7 (1)	36.5 (1)	30.2 (1)
Ni	67 (12)	61 (14)	<140	70 (11)	<160	<160	110 (15)	57 (14)	105 (15)	52 (11)	89 (14)	110 (20)	48 (10)
Cs	<1.1	<1.2	<1.0	0.52 (11)	[0.2]	1.1 (2)	0.79 (15)	0.41 (11)	0.50 (40)	[0.3]	[2]	0.80 (19)	[0.6]
Ba	160 (50)	210 (30)	190 (35)	[200]	nd	230 (30)	290 (40)	nd	nd	[370]	nd	120 (40)	160 (30)
La	23.2 (2)	20.4 (2)	24.5 (2)	13.1 (2)	6.88 (10)	24.1 (2)	20.5 (2)	22.2 (2)	11.7 (1)	26.4 (2)	3.42 (9)	18.6 (2)	20.3 (2)
Ce	55 (1)	52 (1)	65 (1)	30.9 (5)	17.1 (6)	61 (1)	76 (1)	59 (1)	28.4 (7)	71 (1)	8.30 (50)	49 (1)	53 (1)
Nd	39 (2)	37 (2)	42 (2)	22 (2)	13 (1)	40 (3)	52 (3)	38 (2)	18 (3)	41 (2)	7.60(250)	28 (2)	32 (3)
Sm	11.3 (1)	10.5 (1)	12.1 (1)	6.48 (2)	3.83 (2)	11.8 (1)	14.0 (1)	10.8 (1)	6.08 (2)	13.0 (1)	1.90 (2)	9.45 (2)	9.93 (2)
Eu	1.59 (3)	1.31 (3)	1.52 (4)	1.12 (2)	0.73 (4)	1.39 (4)	1.50 (3)	1.39 (4)	1.11 (3)	1.53 (3)	0.50 (3)	1.26 (4)	1.33 (2)
Tb	2.20 (10)	2.10 (10)	2.60 (10)	1.24 (7)	1.10 (10)	2.40 (10)	3.00 (10)	2.10 (10)	1.30 (10)	2.60 (10)	0.46 (7)	1.90 (10)	2.00 (10)
Yb	7.0 (1)	6.6 (1)	7.9 (1)	4.9 (1)	3.8 (1)	7.5 (1)	9.30 (20)	7.20 (10)	5.30 (10)	7.90 (20)	2.30 (10)	5.90 (10)	6.5 (1)
Lu	0.92 (2)	0.92 (2)	0.99 (2)	0.68 (2)	0.52 (2)	1.04 (2)	1.25 (3)	1.96 (2)	0.75 (3)	1.07 (2)	0.29 (2)	0.81 (2)	0.87 (2)
Hf	9.2 (1)	8.3 (1)	9.8 (1)	5.8 (1)	3.4 (1)	9.6 (1)	11.0 (1)	8.4 (10)	5.4 (1)	10.0 (1)	2.0 (1)	7.3 (1)	8.1 (1)
Ta	0.86 (4)	0.92 (5)	1.05 (6)	0.61 (5)	0.42 (5)	1.27 (8)	1.44 (5)	1.05 (7)	0.74 (1)	1.14 (4)	0.42 (5)	0.83 (5)	0.98 (4)
Th	2.5 (1)	1.9 (1)	2.3 (1)	1.6 (1)	1.1 (1)	2.8 (1)	4.6 (1)	2.4 (1)	1.5 (1)	2.5 (1)	0.5 (1)	1.9 (1)	1.9 (1)
U	[4.2]	[1.1]	1.0 (2)	[4.1]	[1.0]	[5.9]	1.6 (3)	[20]	nd	0.8 (2)	[1.8]	[2.5]	[1.2]

TABLE 1. (continued)

PM No.	,1598		,1599	,1604	,1605	,1606	,1607	,1600	,1608	,1609	,1610	,1611	,1612
INAA No.	,1538	,1542	,1546	,1549	,1553	,1556	,1558	,1563	,1568	,1573	,1578	,1582	,1585
Wt (mg)	37.5	18.4	33.1	9.5	25.1	19.7	43.9	34.2	93.8	92.7	112.6	57.8	88.8
SiO_2*	49.3	48.9	48.5	44.7	42.8	48.0	43.7	46.3	48.7	46.4	44.7	44.4	47.7
TiO_2	2.21 (11)	2.41 (12)	1.98 (10)	2.47 (13)	2.56 (40)	2.35 (11)	2.44 (14)	2.41 (11)	2.02 (13)	2.83 (16)	1.87 (15)	2.49 (15)	2.05 (12)
Al_2O_3	12.8 (2)	13.7 (2)	11.7 (2)	11.9 (2)	11.1 (1)	12.5 (2)	14.7 (2)	12.9 (2)	13.6 (2)	12.4 (2)	13.0 (3)	14.0 (2)	13.3 (2)
FeO	15.1 (1)	14.2 (1)	15.8 (1)	17.5 (1)	20.1 (1)	16.0 (1)	16.9 (1)	17.7 (2)	15.3 (1)	18.3 (1)	17.1 (1)	17.2 (1)	16.2 (1)
MnO	0.22 (1)	0.19 (1)	0.24 (1)	0.25 (1)	0.24 (1)	0.23 (1)	0.21 (1)	0.24 (1)	0.22 (1)	0.25 (1)	0.23 (1)	0.23 (1)	0.22 (1)
MgO	8.80 (40)	9.10 (60)	10.8 (40)	11.5 (80)	12.1 (50)	9.30 (50)	9.00 (70)	7.80 (40)	8.50 (40)	9.60 (50)	11.8 (50)	10.9 (6)	8.90 (50)
CaO	10.5 (5)	10.3 (5)	10.2 (4)	10.7 (6)	10.1 (4)	10.5 (5)	12.1 (6)	11.5 (5)	10.6 (5)	9.22 (46)	10.5 (5)	9.79 (54)	10.5 (5)
Na_2O	0.50 (1)	0.60 (1)	0.25 (1)	0.42 (1)	0.46 (1)	0.60 (1)	0.46 (1)	0.62 (1)	0.34 (1)	0.39 (1)	0.26 (1)	0.39 (1)	0.59 (1)
K_2O	0.12 (1)	0.36 (3)	0.06 (1)	0.15 (2)	0.07 (1)	0.15 (2)	0.08 (1)	0.14 (1)	0.06 (1)	0.08 (1)	0.06 (1)	0.05 (1)	0.15 (2)
Sc	55.3 (1)	48.9 (1)	51.9 (1)	57.7 (1)	65.2 (1)	58.3 (1)	62.1 (1)	63.9 (1)	55.4 (1)	59.5 (1)	52.9 (1)	65.7 (1)	59.2 (1)
V	120 (5)	81 (4)	139 (5)	114 (6)	132 (5)	115 (4)	123 (6)	111 (5)	119 (6)	134 (6)	131 (7)	149 (6)	115 (5)
Cr	3210 (10)	2040 (10)	4040 (10)	3160 (10)	3270 (10)	2970 (10)	3490 (10)	3080 (10)	3280 (10)	4040 (10)	3720 (10)	4250 (10)	2790 (10)
Co	33.3 (1)	35.9 (1)	32.5 (1)	36.9 (2)	33.6 (1)	32.0 (1)	41.1 (1)	30.4 (1)	31.7 (1)	35.4 (1)	38.4 (1)	35.8 (1)	30.4 (1)
Ni	110 (20)	nd	nd	170 (25)	80 (20)	78 (15)	75 (10)	76 (13)	50 (12)	70 (11)	73 (13)	<170	<180
Cs	[0.4]	0.7 (14)	0.7 (40)	[0.4]	[0.06]	0.50 (20)	nd	[0.4]	[0.17]	nd	[0.08]	0.56 (13)	[0.4]
Ba	140 (30)	[500]	80 (30)	120 (40)	nd	210 (30)	170 (40)	200 (40)	nd	nd	80 (20)	nd	180 (30)
La	20.1 (2)	39.7 (2)	4.52 (8)	13.2 (1)	3.06 (8)	21.6 (2)	14.1 (1)	28.6 (2)	7.19 (9)	11.7 (1)	5.13 (7)	3.11 (7)	22.3 (1)
Ce	53 (1)	105 (1)	10.4 (8)	31.3 (7)	7.0 (4)	56 (1)	32.1 (4)	69 (1)	19.0 (5)	30 (2)	13.4 (4)	7.0 (6)	58.9 (5)
Nd	34 (2)	62 (3)	7.8 (15)	19 (2)	5.2 (23)	36 (2)	23 (3)	45 (3)	12.9 (13)	18 (2)	8.4 (13)	5.1 (15)	35 (2)
Sm	10.2 (1)	17.6 (1)	2.54 (2)	6.84 (2)	2.14 (2)	10.8 (1)	7.36 (2)	14.2 (1)	3.88 (1)	6.03 (2)	2.85 (10)	2.15 (2)	11.1 (1)
Eu	1.34 (3)	1.78 (4)	0.46 (3)	1.21 (5)	0.6 (3)	1.30 (3)	1.28 (3)	1.60 (3)	0.71 (3)	1.06 (10)	0.59 (3)	0.73 (4)	1.43 (3)
Tb	1.80 (10)	3.80 (10)	0.68 (9)	1.70 (10)	0.46 (8)	2.10 (10)	1.80 (10)	2.80 (10)	0.70 (10)	1.60 (10)	0.79 (9)	0.69 (9)	2.10 (10)
Yb	6.2 (1)	12.2 (2)	2.6 (1)	5.9 (1)	2.9 (1)	6.9 (1)	6.4 (1)	8.7 (2)	3.6 (1)	5.6 (1)	2.9 (1)	2.9 (1)	7.0 (1)
Lu	0.89 (2)	1.59 (3)	0.41 (2)	0.80 (2)	0.42 (2)	0.93 (2)	0.84 (2)	1.13 (2)	0.56 (1)	0.79 (1)	0.46 (1)	0.41 (1)	0.94 (2)
Hf	8.1 (1)	15.4 (1)	2.5 (1)	6.2 (2)	1.5 (1)	9.0 (1)	6.5 (1)	9.9 (1)	3.4 (1)	5.2 (1)	2.3 (1)	2.0 (1)	8.7 (1)
Ta	1.08 (5)	2.02 (7)	0.59 (7)	1.14 (9)	0.37 (5)	1.04 (6)	1.00 (5)	1.10 (4)	0.50 (5)	0.77 (5)	0.38 (5)	0.46 (6)	0.98 (6)
Th	2.0 (1)	7.3 (1)	0.7 (1)	1.9 (2)	<1.5	2.2 (1)	2.0 (1)	3.0 (1)	0.9 (1)	1.5 (1)	0.7 (1)	0.40 (13)	2.1 (1)
U	[2.2]	2.6 (3)	[1.0]	[1.8]	[4.0]	[2.6]	[1.1]	1.4 (3)	[1.9]	[1.5]	[0.2]	[2.2]	1.3 (2)

* = SiO_2 calculated by difference.
[] = uncertain values determined by forced peak integration or counts influenced by undefined interferences; nd = not detected; () = 2 sigma error in last decimal place.

TABLE 2. Whole rock compositions of analyzed VHK basalts; values are in wt% for oxides and in ppm for all other elements.

	14303	14304	14304	14304	14304	14304	14304
PM No.	328	169	177	203	187	189	194
INAA No.	318	168	176	180	148	152	164
Wt (mg)	86.9	26.5	62.8	87.1	115.0	89.5	104.7
SiO_2	†46.0 (2)	†49.0 (2)	†52.1 (3)	†46.6 (2)	*47.4	*48.3	*46.3
TiO_2	1.55 (6)	1.86 (10)	1.07 (8)	2.22 (9)	1.50 (11)	2.27 (13)	5.94 (30)
Al_2O_3	13.6 (8)	16.0 (1)	15.1 (1)	12.0 (1)	14.2 (2)	15.1 (2)	11.9 (2)
FeO	15.1 (2)	10.6 (1)	10.2 (1)	15.8 (2)	15.8 (1)	12.6 (1)	15.8 (1)
MnO	0.23 (2)	0.15 (3)	0.15 (3)	0.28 (3)	0.21 (1)	0.16 (1)	0.17 (1)
MgO	10.8 (1)	9.56 (11)	10.4 (1)	9.80 (8)	10.0 (4)	7.90 (50)	7.20 (40)
CaO	11.6 (1)	10.8 (1)	9.06 (1)	11.0 (1)	9.70 (40)	11.7 (5)	10.0 (5)
Na_2O	0.28 (2)	0.60 (2)	0.60 (1)	0.51 (2)	0.40 (1)	0.56 (1)	0.71 (1)
K_2O	0.46 (3)	0.96 (3)	1.07 (18)	1.22 (3)	0.35 (3)	1.11 (6)	1.71 (12)
P_2O_5	0.04 (2)	0.35 (4)	0.07 (6)	<0.03	na	na	na
Sc	52.4 (6)	29.9 (3)	22.2 (3)	58.7 (7)	52.1 (1)	53.8 (1)	61.5 (1)
V	na	na	na	na	116 (4)	109 (5)	78 (6)
Cr	3190 (40)	1262 (16)	1153 (15)	3450 (40)	3530 (10)	2560 (10)	2040 (10)
Co	37.5 (4)	20.2 (2)	15.8 (19)	32.6 (4)	34 (1)	36.5 (1)	34.9 (1)
Ni	100 (20)	170 (20)	79 (14)	nd	<120	130 (15)	93 (12)
Rb	14 (2)	28 (2)	43 (2)	38 (3)	na	na	na
Sr	100 (30)	156 (20)	217 (15)	130 (30)	na	na	na
Cs	0.54 (6)	1.31 (5)	1.86 (4)	0.27 (5)	0.36 (8)	1.70 (1)	2.20 (1)
Ba	252 (15)	920 (20)	1160 (20)	202 (14)	60 (20)	560 (40)	820 (40)
La	7.07 (9)	51.4 (6)	25.2 (3)	6.11 (8)	3.33 (18)	20.5 (2)	50.6 (2)
Ce	20 (9)	135 (18)	66 (1)	16.8 (5)	8.5 (3)	50 (1)	126 (1)
Nd	13 (4)	78 (6)	41 (4)	12 (2)	4.5 (5)	30 (1)	83 (3)
Sm	3.86 (6)	23.7 (4)	12.1 (2)	3.74 (6)	1.78 (2)	9.66 (2)	26.6 (1)
Eu	0.69 (2)	2.30 (4)	3.02 (5)	0.74 (2)	0.68 (2)	1.35 (3)	2.56 (3)
Tb	0.92 (4)	5.13 (10)	2.82 (6)	0.89 (4)	0.37 (7)	2.00 (10)	5.60 (10)
Yb	3.71 (6)	22.6 (3)	16.8 (2)	4.08 (7)	2.03 (5)	7.70 (10)	19.6 (2)
Lu	0.56 (1)	3.14 (6)	2.56 (4)	0.61 (1)	0.30 (1)	1.03 (2)	2.57 (3)
Zr	110 (30)	730 (100)	780 (80)	70 (30)	na	na	na
Hf	2.82 (8)	18.7 (3)	21.3 (3)	3.00 (9)	1.60 (10)	7.10 (10)	18.9 (1)
Ta	0.33 (2)	2.44 (5)	2.53 (5)	0.59 (3)	0.31 (4)	1.11 (6)	3.30 (6)
Th	1.21 (5)	10.9 (2)	11.4 (2)	0.92 (5)	0.62 (6)	3.20 (1)	5.20 (1)
U	0.44 (5)	3.26 (11)	4.79 (15)	0.14 (5)	[0.6]	1.30 (10)	3.20 (30)

* = SiO_2 calculated by difference.
† = major elements determined by electron microprobe analysis of fused glass bead.
[] = uncertain values determined by forced peak integration or counts influenced by undefined interferences; nd = not detected; na = not analyzed; ( ) = 2 sigma error in last decimal place.

constraint and will not be considered further. Generally, those basalts with the most primitive REE profile contain the greatest abundances of the compatible and lowest abundances of incompatible elements. Positive correlations between the HFS elements and La/Lu and Sm/Eu ratios are noted.

VHK basalts

Major and rare earth elements. As documented by previous authors (i.e., *Shervais et al.*, 1985b; *Goodrich et al.*, 1986; *Warren et al.*, 1986; *Neal et al.*, 1988b), major element compositions of VHK basalts (Table 2) are similar to HA basalts (Table 1). However, the seven new VHK basalts studied here have MG#'s (44.8-64.6) that exceed the upper limit of the range defined by the HA basalts. A similar situation is noted with Al_2O_3 (11.9-16.0 wt.%). The Na, Ca, and Ti abundances in these VHK basalts are similar to those of HA basalts (0.28-0.71 wt.% Na_2O; 9.06-11.7 wt.% CaO; 1.55-2.27 wt.% TiO_2), except the elevated TiO_2 content of 14304,194(164) (5.94 wt.%). As indicated by the classification of these basalts, K_2O is generally elevated above abundances in HA basalts. In the seven new samples, K_2O ranges from 0.35-1.71 wt.%. The analyses of fused glass beads by electron microprobe included P_2O_5, which ranges from <0.03-0.35 wt.%. The major-element compositions of the VHK basalts have also been plotted on an Ol-An-Qz pseudoternary (Fig. 3). As with previously reported VHK basalts, these plot around the Ol-Plag cotectic and are similar to HA basalts.

The REE abundances in the seven new VHK basalts (Table 2) exhibit a wide range, from 3.33 ppm to 51.4 ppm La. Generally, there is a negative Eu anomaly [$(Sm/Eu)_N$ = 1.51-3.91], except for 14304,187(148), which exhibits practically no Eu anomaly (Fig. 4a). The profile of this sample is almost flat, with a slight depression in the MREE. Unlike the HA basalts, the profiles exhibit either a flattening of the HREE, or an increase from the MREE to the HREE [e.g., (Fig. 4a)]. These profiles, which are concave upward, appear similar to lunar granites (Fig. 4b), consistent with the assimilation of granite in VHK basalt petrogenesis (e.g., *Shervais et al.*, 1985b; *Neal et al.*, 1988b).

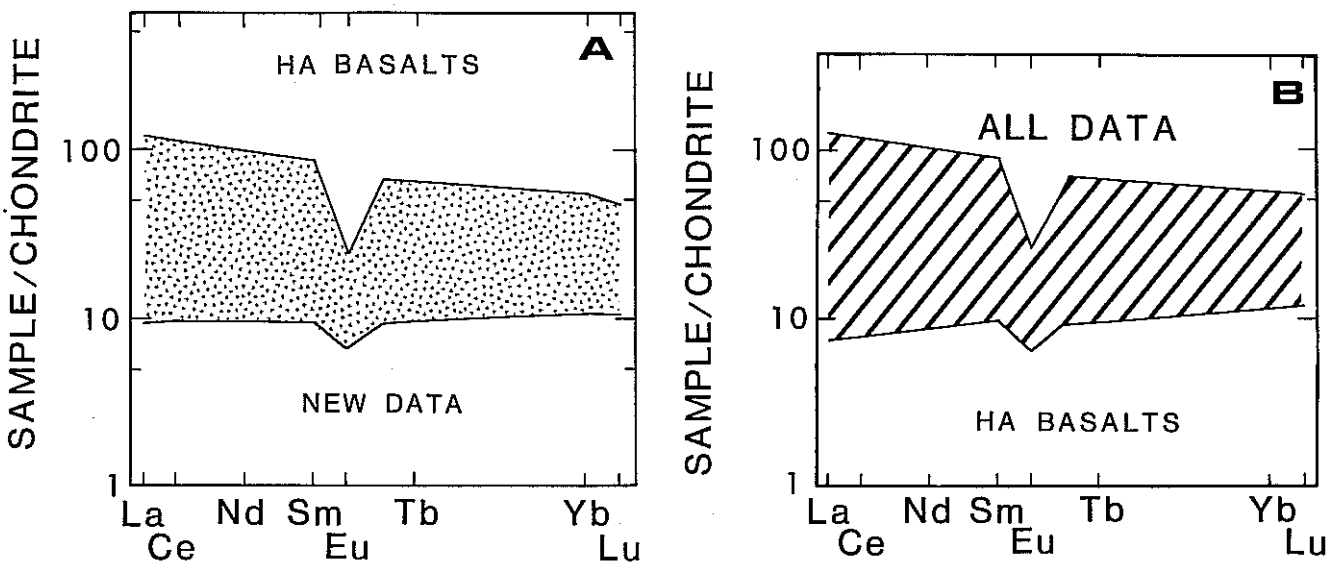

Fig. 2. **(a)** The range of chondrite-normalized REE profiles for the 22 new HA basalts. **(b)** All Apollo 14 HA basalt REE profiles represented on a chondrite-normalized plot. Data are from *Dickinson et al.* (1985), *Shervais et al.* (1985a), *Neal et al.* (1988a), and this study.

Trace elements. Generally, the ranges in compatible, LIL, and HFS elements (Table 2) expand those previously reported for VHK basalts (e.g., *Shervais et al.*, 1985b; *Neal et al.*, 1988b). Vanadium was only determined in three basalts from breccia 14304 (Table 2), and Rb, Sr, and Zr were determined only on the remaining four VHK basalts of our study. Barium abundances are generally higher than HA basalts, except for 14304,187(148), which contains only 60 ppm Ba. This is the lowest Ba abundance yet reported from VHK basalts, which are usually characterized by elevated Ba contents (e.g., *Shervais et al.*, 1985b). The classification of this sample as "VHK" is supported by the Ba/La ratio (18.0), which is within the range defined by the other six VHK basalts (17.9-46.0). It also has low REE abundances, comparable to a primitive HA basalt, which would contain between 25-30 ppm Ba. Therefore the Ba content of 14304,187(148) is elevated relative to a comparable HA basalt; coupled with the high K/La ratio (872), this sample is classified as a VHK basalt.

DISCUSSION

HA Basalts

The analyses of "new" basalts obtained by breccia pull-apart efforts have enabled a uniform approach to be developed for basalt petrogenesis at the Apollo 14 site. The range in trace-element compositions of the HA basalts has led previous authors to suggest the presence of various groups of basalts (defined by a limited data set). The petrogenesis of these groups of basalts required derivation from different source regions (*Shervais et al.*, 1985a; *Dickinson et al.*, 1985). However, *Neal et al.* (1988a) proposed a combined assimilation (of KREEP) and fractional crystallization (AFC) model (after *DePaolo*, 1981) in order to generate all HA basalts at the Apollo 14 site. We do not envisage that every analyzed clast represents a separate HA basalt flow. The compositional variability within the HA basalt suite may be a function of the inhomogeneity of the parental melt in the magma chamber. For example, the edges of the magma chamber will contain a higher proportion of assimilated wallrock than the center.

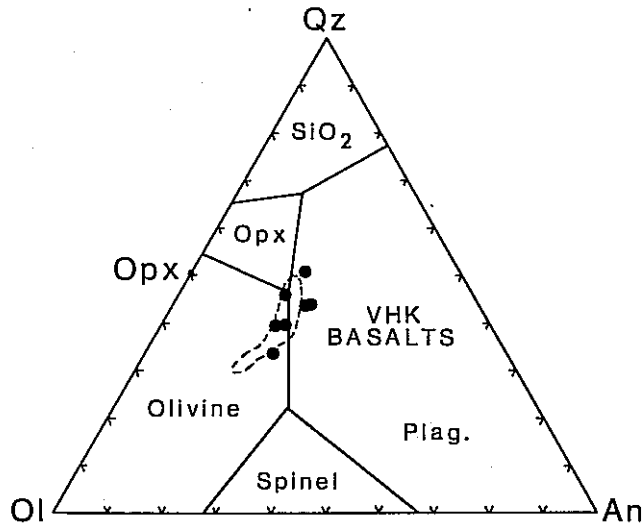

Fig. 3. Major-element compositions of the VHK basalts represented on an Ol-An-Qz pseudoternary (after *Walker et al.*, 1972, 1973). The dashed field is for HA basalts (*Dickinson et al.*, 1985; *Shervais et al.*, 1985a; *Neal et al.*, 1988a). Phase boundaries are drawn for Fe/(Fe+Mg) = 0.6 (see *Neal et al.*, 1988a).

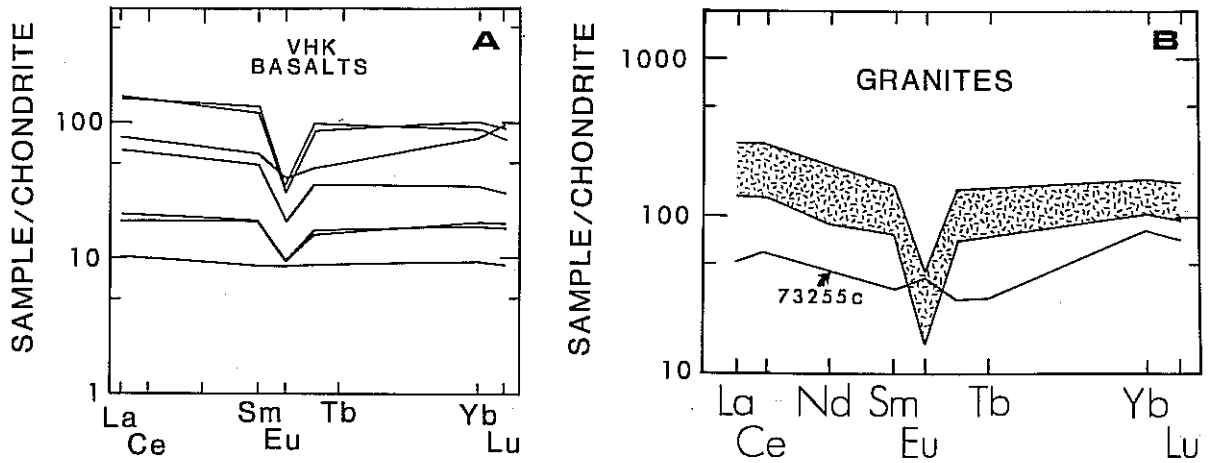

Fig. 4. (a) Chondrite-normalized REE profiles for the seven new VHK basalts. (b) Chondrite-normalized REE profiles of lunar granite.

Eruption to the surface can initially draw magma from the edge of the chamber before the center. Therefore it is possible for one flow to grade from primitive to evolved, depending on heterogeneity in the magma chamber and rate of extrusion. The range in textures of HA basalts (*Neal et al.*, 1989) is more restricted than the range in whole-rock compositions. The textures could easily represent different regions of the same basalt flow. Observed textures do not correlate with observed ranges in trace-element abundances, although more evolved basalts (i.e., Ca- and Fe-rich pyroxene compositions) generally contain higher abundances of incompatible trace elements.

KREEP was chosen as the modeled assimilant because of the similarity between the REE patterns from evolved HA basalts and KREEPy lithologies. With new data, *Neal et al.* (1988a) demonstrated that a continuum of basalt compositions existed, rather than the groups proposed by *Shervais et al.* (1985a) and *Dickinson et al.* (1985). This removed the need to invoke different source regions for basalts of different compositions. However, possible gaps in the continuum still exist (Fig. 5), and the most ardent opponents of AFC may still advocate the presence of two basalt groups.

As the new HA basalts have major element compositions similar to those previously reported (Fig. 1), we have used the same crystallization parameters (as reported in *Neal et al.*, 1988a). *DePaolo* (1981) contends that major elements in an AFC process can be essentially modeled by fractional crystallization alone. Therefore, we assume that the assimilant has little effect on the major elements in our model, modeling these elements by fractional crystallization. Olivine and chromite are the first phases to crystallize (*Walker et al.*, 1972). By using the lever rule (Fig. 1), only olivine (90%) and chromite (10%) fractionate during the first 14% crystallization. This is consistent with the petrography described in part 1 of this contribution (*Neal et al.*, 1989), where olivine phenocrysts with chromite inclusions are present either with or without pyroxene reaction rims. After 14% crystallization, the olivine-plagioclase cotectic is reached, and plagioclase (50%) fractionates with olivine (40%) and chromite (10%) until 21% of the parental liquid has crystallized. At this point, the olivine-opx-plagioclase peritectic is reached, and olivine fractionation ceases with orthopyroxene becoming the dominant liquidus phase. In our model, we envisage that all olivine has been effectively removed and no appreciable back reaction occurs at the onset of pyroxene crystallization. This is an oversimplification, as pyroxene reaction rims around olivine are present, especially in the ophitic HA basalts (*Neal et al.*, 1989). However, this approach is reasonable for demonstrating the applicability of our model. Plagioclase (30%), orthopyroxene (60%), and ilmenite (10%) are the crystallizing phases until 70% of the parental liquid is solidified.

We do not consider that 70% crystallization is too high, especially as some lunar basalts contain evidence of silicate liquid immiscibility (SLI) in the mesostasis. In order to achieve the magma composition necessary for SLI, crystallization must normally be >90% (e.g., *Hess et al.*, 1975).

Realistic crystallizing conditions were recreated by calculating the Fo content of fractionating olivine iteratively, in crystallization increments of 2% using the Mg/Fe ratio of the resultant liquid (method of *Longhi*, 1977). This yielded a range of olivine compositions from Fo77.0 to Fo67.4 throughout the period that olivine was on the liquidus. This does not cover the Fe-rich portion of the measured range of olivine compositions reported in part 1 of this study (*Neal et al.*, 1989), but covers most of the core compositions. The zonations in olivine are a function of the nucleation density and growth rate of olivine from the melt, both dependent upon cooling rate, whereas the core compositions (earliest olivine) are a direct function of melt composition. During the first 7% of plagioclase fractionation (up to the peritectic), a composition of An92 was used. Although more calcic plagioclases are present in these HA basalts (*Neal et al.*, 1989), this composition represents the average composition over this crystallization period. After the peritectic, a plagioclase of composition An79 was fractionated. Such compositions were

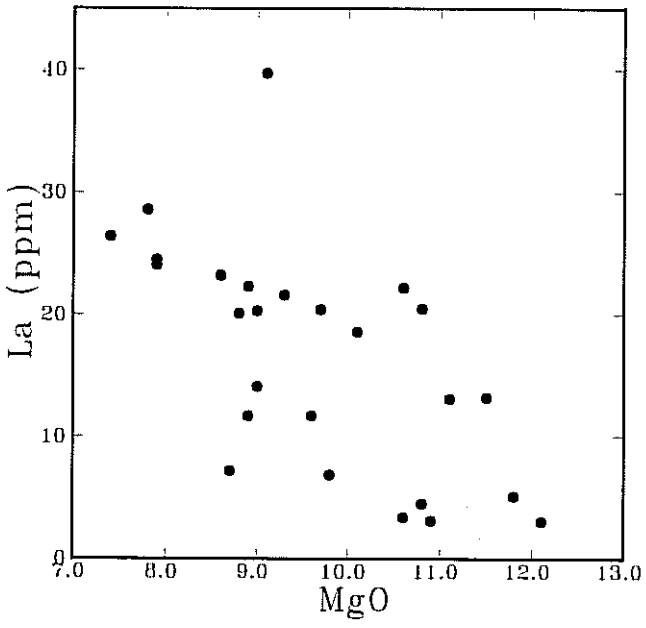

Fig. 5. Lanthanum (ppm) vs. Hf (ppm) for Apollo 14 HA basalts. Fields represent previously reported HA compositions and points, the new HA data from this study. The calculated AFC path is between parental basalt 14321,1422 (*Neal et al.,* 1988a) and KREEP (*Vaniman and Papike,* 1980). Tick marks represent the percentage of magma remaining.

based upon the zonation observed in mare basalt plagioclases (*Neal et al.,* 1989). The compositions of chromite (MG# = 12.6) and ilmenite (MG# = 9,4) were estimated from analyzed 14321 basalts (*Neal et al.,* 1988a, 1989), and these were kept constant throughout. Pyroxene compositions in a crystallizing magma will evolve from Mg-rich to Ca- and Fe-rich. An average pyroxene composition of Mg# = 48 is used. This is permissible, since olivine fractionation has already depleted the magma in Mg.

Results of this modeling are presented in Table 4. The calculated crystallization path accounts for all the new Apollo 14 high-Al mare basalt data presented in this study. The major element modeling above allows the proportions of crystallizing phases to be derived. These are now used in the trace element modeling. The modeling of the new HA basalts is conducted using the same KREEP composition as in *Neal et al.* (1988a) (15386 "IKFM": *Vaniman and Papike,* 1980). This is taken as a representative KREEP sample.

In the model calculations, the mass assimilated/mass crystallized (the "r" value in equation (6a) of *DePaolo,* 1981) was first estimated as 0.2 by studying the compositions of the parental basalt and assimilant. As this is basically a basalt-basalt interaction, the r value will be low. The r value of 0.2 was then adjusted slightly in order that the derived AFC path passed through all HA basalt compositions. This resulted in an r value of 0.22. The partition coefficients used in our calculations are presented in Table 3.

In Fig. 5, La is plotted against Hf for all Apollo 14 HA basalts. This diagram was used by *Dickinson et al.* (1985) to demonstrate the presence of five distinct Apollo 14 basalt groups. Previously reported HA basalt compositions (from *Dickinson et al.,* 1985; *Shervais et al.,* 1985a; *Neal et al.,* 1988a) are presented as fields (as they will be in subsequent diagrams), and it is evident that two fields exist. The new basalt data go some way toward "closing the gap" on this plot. This is also illustrated in Fig. 2b, where a continuous range of REE patterns is depicted for Apollo 14 HA basalts. An AFC path has been calculated (using equation 6a of *DePaolo,* 1981) between basalt 14321,1422 (taken as parental because of low incompatible trace element abundances and SiO_2, and high MG#) and IKFM KREEP (Fig. 5). The AFC model must be extended in order to accommodate the new data, and in all subsequent diagrams, the AFC path is calculated to 70% crystallization of the parent and 15.4% KREEP assimilation (r = 0.22). Results of the AFC modeling, along with the parental magma and assimilant compositions, are presented in Table 4.

The AFC model can be used to generate an array of REE patterns between the parental basalt and KREEP (Fig. 6). This approach is feasible as the new data, combined with that in the literature, give a continuum of REE profiles (Fig. 2b). The gaps present in the REE profiles of HA basalts from Fig. 6 of *Neal et al.* (1988a) have largely been filled. Dashed lines represent the parent and most evolved HA basalt yet analyzed. Further evidence that the new HA basalt data conform with the proposed AFC model is seen in Figs. 7 a,b. In these diagrams (La vs. Sc/Sm and Ta vs. Sm/Eu), the new data plot in approximately the same relative positions in Fig. 7 as in Figs. 5 and 6. The extension of the model to 70% fractional crystallization is also supported by these diagrams.

The major elements do not appear to fit in as well as the trace elements in our AFC model. For example, as noted above, the sample with the highest La abundance does not contain the lowest MgO. However, although large errors are associated with the MgO analyses (≈±0.5 wt.%), a broad negative

TABLE 3. Crystal/liquid partition coefficients.

	Olivine	Pyroxene	Plagioclase	Chromite	Ilmenite
K	0.0068	0.014	0.17	0	0
Ba	0.03	0.013	0.686	0.005	0.005
Hf	0.04	0.063	0.05	0.38	1.817
Th	0.03	0.13	0.05	0.55	0.55
Sc	0.4	1.6	0.065	1.5	1.5
La	(0.0001)	(0.012)	0.051	0.029	0.029
Ce	0.0001	0.038	0.037	0.038	0.038
Sm	0.0006	0.054	0.022	0.053	0.053
Eu	0.0004	0.1	1.22	0.02	0.02
Yb	0.02	0.671	0.012	0.39	0.39
Lu	(0.02)	0.838	0.011	0.47	0.47

Brackets indicate estmiated partition coefficient.
References: *Arth and Hanson* (1975); *Binder* (1982); *Dostal et al.* (1983); *Drake and Weill* (1975); *Haskin and Korotev* (1977); *Irving and Frey* (1984); *McKay and Weill* (1976); *McKay et al.* (1986); *Schnetzler and Philpotts* (1970); *Villemant et al.* (1981).

TABLE 4. Modeling results for HA basalts (oxides in wt.%, elements in ppm).

		Proportion of Liquid Remaining								
	Parent	0.95	0.9	0.86	0.79	0.7	0.6	0.5	0.4	0.3	KREEP
SiO_2	46.1	46.8	47.6	48.3	49.1	49.2	49.4	49.6	49.9	50.3	50.8
TiO_2	2.73	2.59	2.44	2.31	2.09	2.14	2.21	2.30	2.42	2.65	2.23
Al_2O_3	11.3	11.9	12.5	13.1	12.8	12.8	12.8	12.9	12.9	12.9	14.8
FeO	17.9	17.4	16.9	16.4	16.5	16.4	16.3	16.1	16.0	15.8	10.6
MnO	0.23	0.23	0.22	0.22	0.23	0.24	0.26	0.28	0.30	0.32	0.16
MgO	11.1	9.86	8.52	7.34	6.75	6.67	6.58	6.45	6.29	6.05	8.17
CaO	10.1	10.7	11.2	11.8	11.9	11.9	11.9	11.8	11.8	11.6	9.71
Na_2O	0.48	0.51	0.53	0.56	0.57	0.54	0.52	0.49	0.45	0.40	0.73
La	3.19	4.60	6.16	7.54	9.86	13.5	18.1	25.0	31.7	42.5	83.5
Ce	9.30	12.9	16.9	20.5	26.4	35.8	47.4	64.6	81.8	110	211
Sm	2.10	2.77	3.51	4.16	5.26	6.96	9.06	12.2	15.2	20.5	37.5
Eu	0.62	0.69	0.77	0.84	0.91	1.04	1.19	1.37	1.60	1.87	2.75
Yb	3.02	3.53	4.09	4.59	5.43	6.42	7.59	8.98	10.7	14.4	24.4
Lu	0.44	0.51	0.59	0.66	0.78	0.91	1.05	1.32	1.43	1.69	3.40
Sc	64.1	65.6	67.2	68.6	71.9	69.3	66.5	63.5	60.2	56.7	23.6
Ta	0.45	0.54	0.63	0.71	0.85	1.06	1.31	1.63	2.03	2.65	4.60
Hf	1.70	2.25	2.86	3.39	4.29	5.59	7.17	10.3	11.6	14.9	31.6
Th	0.20	0.36	0.53	0.68	0.94	1.33	1.82	2.42	3.21	4.27	10.0
% Crystallized	0-14	15-21	22-70								
Olivine	90	40	0								
Plagioclase	0	50	30								
Pyroxene	0	0	60								
Ilmenite	0	0	10								
Chromite	10	10	0								

References: *Neal et al.* (1988a); *Vaniman and Papike* (1980).

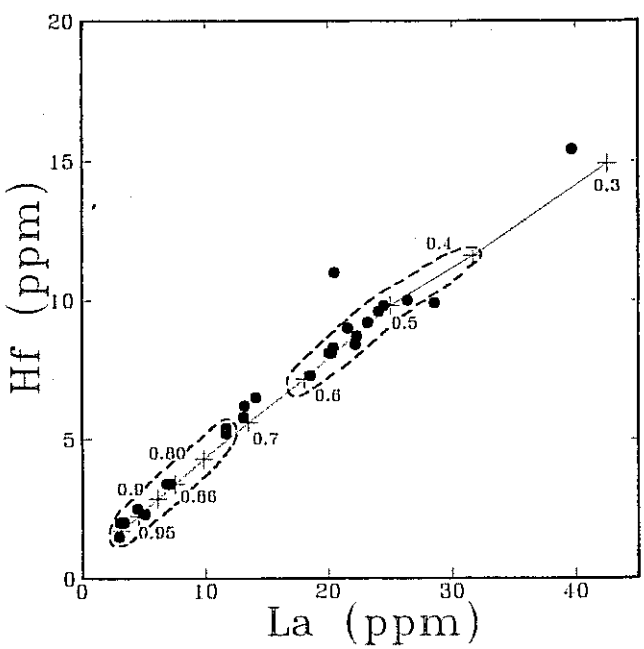

Fig. 6. Chondrite-normalized plot for the REE generated by the AFC model (Table 4) for HA basalt compositions. Values represent amount crystallized/amount assimilated.

correlation exists between MgO and La (Fig. 8), indicative of fractional crystallization. However, our model requires an AFC process to generate the range of HA basalt compositions. We consider that the assimilant does exert an effect upon the major elements, and modeling these by fractional crystallization alone may be an oversimplification. *Shih* (1977) noted an inverse correlation between MG# and incompatible elements in KREEP basalts, the opposite of what is expected. Therefore prolonged assimilation of a KREEP basalt composition could increase the MgO content of the residual magma, while also increasing the incompatible elements. Although MgO and La have a broad negative correlation, such a scenario could account for the dispersion in the MgO data.

VHK Basalts

Since the discovery, characterization, and definition of VHK basalts (*Warner et al.*, 1980; *Shervais et al.*, 1985b), it has been hypothesized that granite assimilation by a HA basalt has been the key to their petrogenesis (*Shervais et al.*, 1985b; *Shih et al.*, 1986). However, the unusually low HFS elements in VHK basalts would appear to negate this theory. *Shervais et al.* (1985b) and *Warren et al.* (1986) proposed that preferential assimilation of granitic feldspars would overcome this problem, and still yield a VHK composition. *Neal et al.* (1988b) proposed an AFC process (after *DePaolo*, 1981), involving lunar granite and a HA magma, in order to generate VHK basalts. This model generates the low HFS element concentrations, as well as the high LIL element abundances. Assimilation

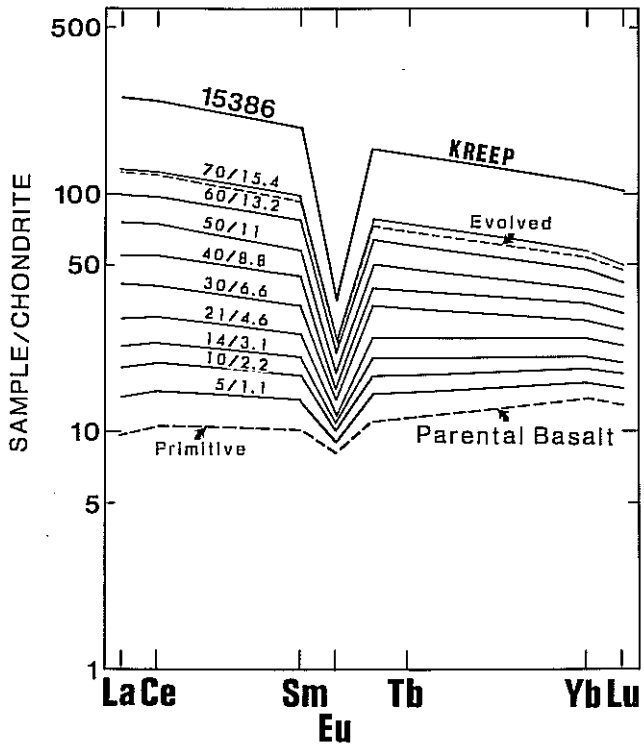

Fig. 7. **(a)** Lanthanum (ppm) vs. Sc/Sm. The calculated AFC path is again between the parental basalt 14321,1422 and KREEP. Abundances are given in Table 4. The field in both A and B represent previously reported HA basalt compositions. Tick marks represent the percentage of magma remaining. **(b)** Tantalum (ppm) vs. Sm/Eu, illustrating the applicability of the AFC model. Tick marks represent the percentage of magma remaining.

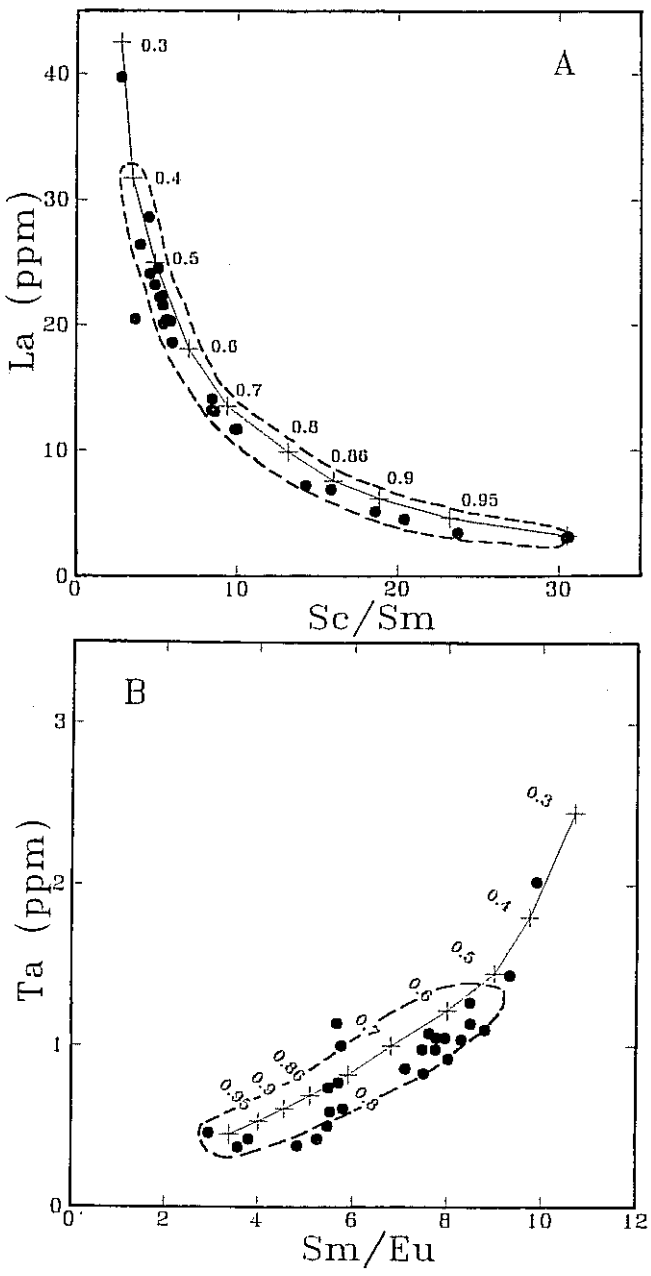

Fig. 8. Lanthanum (ppm) vs. MgO (wt.%) for the "new" HA basalts.

of granite is supported by the presence of K-feldspar and K-rich glass in VHK basalts (*Neal et al.*, 1989). Such K-rich compositions cannot be generated from a HA basalt by fractional crystallization alone. One surprising outcome of this approach was that no one parental HA basalt can generate all VHK compositions. This argues not only for more than one VHK basalt flow, but also a KREEP component in the VHK compositions. This is necessary because more evolved HA basalts are required as parental magmas for some VHK compositions.

The VHK basalts fall between HA basalts and lunar granites on trace-element plots. In Figs. 9–11, all VHK data are plotted as points, and Apollo 14 HA mare basalts and lunar granites are plotted as fields. For the purposes of illustration, three parental HA compositions are used in the AFC calculations: (1) primitive (14321,1161 of *Shervais et al.*, 1985a); (2) intermediate (14321,1443 of *Neal et al.*, 1988a); and (3) evolved (14321,1542, this study). These compositions (Table 5) span the entire range of Apollo 14 HA basalts. The fractionating phases are kept the same as reported in *Neal et al.* (1988b), as major-element compositions of the new VHK basalts are similar to those previously reported (Fig. 3). The r value of 0.5 is the same as in this previous study. This higher value is required because granite has a lower melting point than basalt. The partition coefficients used are given in Table 3. As an extension of the model proposed by *Neal et al.* (1988b), we have used not only an average granite and composition 73255c (trace element poor) as assimilants, but also felsite 12033,517 (trace element rich) of *Warren et al.*

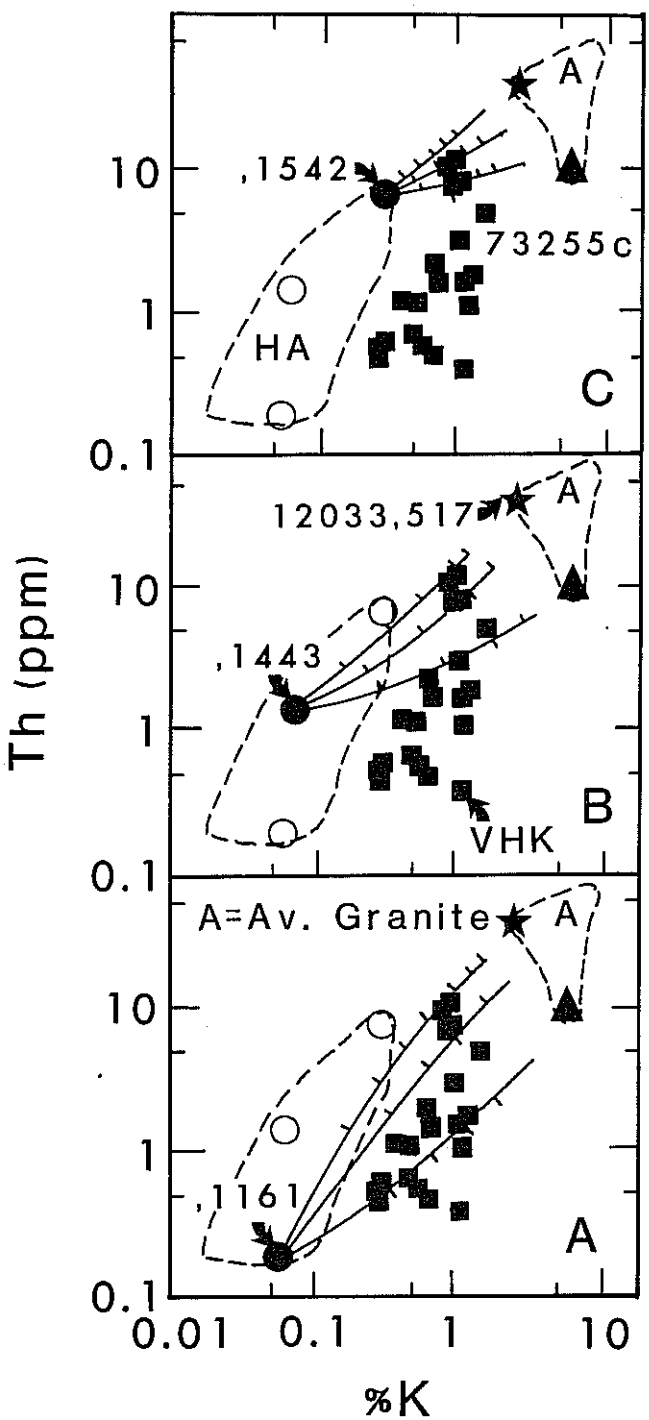

Fig. 9. Percent K vs. La (ppm) for HA and VHK basalts, and lunar granite. AFC paths have been calculated (tick marks represent 5% increments of fractional crystallization—2.5% granite assimilation) between the parental HA basalts and granite assimilants 12033,517, average granite, and 73255c. A: HA basalt 14321,1161 is taken as parental; B: HA basalt 14321,1443 is taken as parental; C: HA basalt 14321,1542 is taken as parental.

(1987). This approach allows the compositional variability of lunar granite to be accounted for in our model for VHK basalt petrogenesis. Results of AFC modeling for VHK basalt petrogenesis are presented in Table 6.

Figure 9 is of La (ppm) vs. %K, a classic plot for VHK basalts. The diagram has been split into three parts in order to clearly demonstrate the calculated AFC paths (using equation 6a of *DePaolo,* 1981) between each parental basalt and granite assimilant. In Fig. 9a, basalt 14321,1161 is taken as parental. An interesting feature of this plot is that all VHK basalt compositions cannot be generated from this parent magma and one granite composition as the assimilant. In order to generate VHK basalts with high La abundances, ,1161 must assimilate a granite similar to 12033,517, whereas in order to generate those VHK basalts with lowest La abundances, ,1161 must assimilate a granite similar to 73255c. It is possible to generate those containing intermediate La abundances by ,1161 assimilating a granite similar to the average composition. However, in order for magma ,1161 to generate VHK basalts with high La abundances, it must assimilate up to 17.5% of granite 12033,517 (Fig. 9a). Such a large amount of granite assimilation will dramatically affect the major element composition of the resulting VHK basalt (i.e., the major elements would no longer be dominated by the parental basalt; elements such as Si and Al would be greatly affected). In order for granite to not adversely affect the major element compositions of VHK basalts, a maximum of only 10% can be incorporated. Therefore, basalt ,1161 cannot be parental to VHK basalts with high La abundances. However, it may reasonably be considered parental to VHK basalts with intermediate and low La abundances, as these compositions can be generated by a maximum of only 8% assimilation of average granite and 73255c, respectively (Fig. 9a).

In Fig. 9b the VHK basalts with intermediate La abundances are better represented by using basalt 14321,1443 as the parental magma and either the composition of average granite or 73255c. A maximum of 7% assimilation of average granite or 73255c is required to generate these VHK basalts. The VHK basalts containing the highest abundances of La are generated by using basalt 14321,1542 as the parental magma assimilating a maximum of 7.5% average granite or 73255c (Fig. 9c).

In Fig. 10 Th (ppm) is plotted against %K, an element difficult to model for VHK basalt petrogenesis (e.g., *Shervais et al.,* 1985b). As in Fig. 9, this diagram has been divided into three parts. Using the 10% maximum as a reasonable upper limit for granite assimilation in VHK basalt petrogenesis, a similar picture is defined as in Fig. 9. All VHK compositions with low and intermediate Th abundances can be adequately modeled using parental basalt ,1161 and granite 73255c and average granite, respectively (Fig. 10a). For VHK basalts with low Th abundances, 8% assimilation of 73255c is required. For those with intermediate Th abundances, 8% assimilation of average granite is required. However, those VHK basalts with intermediate Th abundances are better represented by our AFC model if basalt ,1443 is the parental magma and granite 73255c is the assimilant (Fig. 10b). A maximum of 7.5% granite assimilation is required to generate these VHK compositions. The highest Th abundances (Fig. 10c) are

TABLE 5. Modeling parameters for VHK basalts (ppm).

	Parental Magmas			Assimilated Granite		
	,1161	,1443	,1542	73255c	Avg. Granite	12033,517
K	564	747	2989	62665	58864	24905
Ba	32	130	230	5470	4490	4540
Hf	1.78	5.43	15.4	16.0	15.4	36.8
Th	0.20	1.50	7.30	9.50	42.3	40.0
Cr	3660	3485	2040	70	414	480
La	2.89	13.5	39.7	20.3	50.7	82.0
Ce	8.40	35.0	105	50.0	123	199
Sm	2.11	7.59	123	6.74	16.7	27.7
Eu	0.56	1.12	1.78	2.71	2.52	3.10
Yb	2.89	6.33	12.2	10.3	24.7	36.7
Lu	0.47	0.91	1.59	1.50	3.71	5.80

References: *Shervais et al.* (1985a); *Neal et al.* (1988a); *Blanchard et al.* (1977); *Blanchard and Budahn* (1979); *Quick et al.* (1977); *Warren et al.* (1983); *Salpas et al.* (1985).

generated between the parental basalt ,1542 assimilating up to 7.5% of either average granite or 73255c (as for La in Fig. 9c).

When Hf (ppm) is plotted against %K (Fig. 11), a similar scenario is witnessed as in Figs. 9 and 10. Very high potassium basalts with low Hf abundances can be generated by a maximum of 7% granite assimilation (either 73255c or average granite) by parental basalt ,1161 (Fig. 11a). Very high potassium basalts with intermediate Hf abundances cannot be modeled by this parental magma, but can be generated by using parental basalt ,1443. A maximum of 7% granite assimilation (either average granite or 73255c) is required (Fig. 11b). Basalts with high Hf abundances are generated by parental basalt ,1542 assimilating 7.5% of either 73255c or average granite (Fig. 11c).

The fact that there is a slight variation (±1%) in the amount of required granite assimilation for different elements in VHK basalts of low, intermediate, or high incompatible element concentrations is not a problem. Such a small variation is well within error of the AFC calulation. Another outcome of our modeling is that VHK basalts with low, intermediate, or high incompatible element abundances are generated by primitive, intermediate, and evolved parental magmas, respectively. Although VHK basalts with intermediate La and Th concentrations can be modeled by parental basalt ,1161, Fig. 10 demonstrates this is not the case for Hf abundances. The "paralleling" of the VHK basalt with parental HA basalt (i.e., low incompatible element VHK basalts = primitive HA basalt parent, etc.) leads us to conclude that the parental magma not only dominates the major elements, but also the trace-element

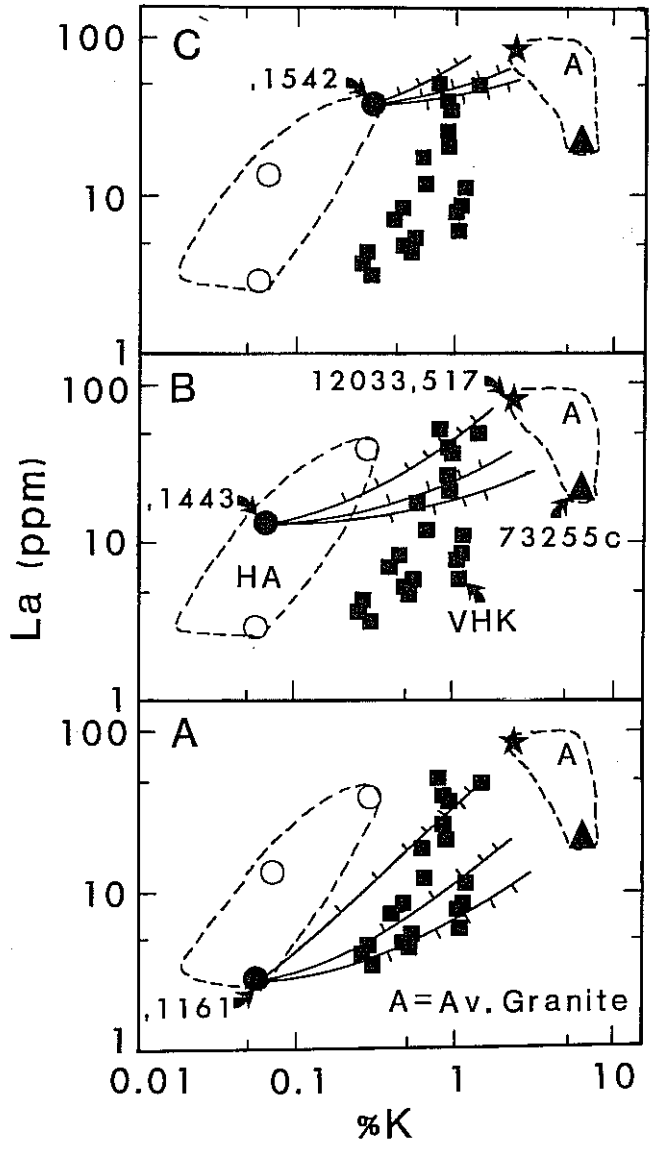

Fig. 10. Percent K vs. Th (ppm) for HA and VHK basalts, and lunar granite. The AFC paths have been calculated (tick marks represent 5% increments of fractional crystallization—2.5% granite assimilation) between the parental HA basalts and granite assimilants 12033,517, average granite, and 73255c. A: HA basalt 14321,1161 is taken as parental; B: HA basalt 14321,1443 is taken as parental; C: HA basalt 14321,1542 is taken as parental.

TABLE 6. Modeling results (ppm) for VHK basalts.

F Value	K	Ba	Hf	Th	Cr	La	Ce	Sm	Eu	Yb	Lu
					1161/Average Granite						
0.95	3690	312	2.67	2.43	3480	5.71	15.3	3.10	0.72	4.32	0.69
0.90	7162	614	3.64	4.88	3301	8.84	23.0	4.20	0.90	5.90	0.92
0.85	11039	898	4.73	7.59	3147	12.3	31.6	5.42	1.10	7.66	1.19
0.80	15398	1298	5.94	10.6	3091	16.3	41.3	6.80	1.33	9.62	1.48
					1161/73255c						
0.95	3890	321	2.70	0.71	3463	4.11	11.8	2.57	0.73	3.57	0.57
0.90	7584	641	3.71	1.26	3266	5.46	14.9	3.09	0.92	4.31	0.68
0.85	11709	998	4.83	1.88	3096	6.98	18.7	3.67	1.14	5.14	0.80
0.80	16347	1398	6.08	2.57	3023	8.68	23.0	4.31	1.38	6.06	0.94
					1161/12033,517						
0.95	1904	272	3.79	2.31	3483	7.36	19.3	3.68	0.75	4.95	0.80
0.90	3391	538	6.00	4.62	3307	12.3	31.4	5.42	0.97	7.25	1.16
0.85	4995	821	8.39	7.12	3157	17.7	44.6	7.30	1.19	9.68	1.54
0.80	6532	1070	10.7	9.54	3104	22.9	57.4	9.10	1.33	12.1	1.92
0.75	8144	1336	13.0	12.0	2426	28.4	70.7	11.1	1.49	14.2	2.23
0.70	9901	1624	15.3	14.7	1770	34.5	85.2	13.1	1.67	16.2	2.52
0.65	11850	1938	17.9	17.6	1275	41.0	101	15.4	1.86	18.4	2.84
0.60	14024	2282	20.7	20.8	907	48.5	119	18.0	2.07	20.7	3.16
					1443/Average Granite						
0.95	3863	364	6.48	3.78	3421	16.8	43.2	8.85	1.24	7.92	1.15
0.90	7154	608	7.51	6.16	2828	20.3	52.1	10.2	1.36	9.39	1.36
0.85	10684	868	8.55	8.67	2064	24.1	61.4	11.6	1.51	10.8	1.55
0.80	14595	1151	9.68	11.4	1485	28.3	71.8	13.2	1.66	12.2	1.74
					1443/73255c						
0.95	4063	415	6.51	2.06	3404	15.2	39.4	8.33	1.25	7.17	1.03
0.90	7561	711	7.57	2.64	2799	17.0	44.2	9.10	1.39	7.87	1.12
0.85	11316	1027	8.65	3.25	2027	19.0	49.1	9.92	1.54	8.46	1.19
0.80	15476	1371	9.82	3.93	1442	21.2	54.6	10.8	1.71	9.09	1.27
					1443/12033,517						
0.95	2084	367	7.60	3.66	3425	18.5	47.2	9.43	1.27	8.55	1.26
0.90	3497	614	9.80	5.91	2834	23.8	60.1	11.4	1.43	10.7	1.57
0.85	5013	876	12.1	8.29	2071	29.4	73.9	13.4	1.61	12.7	1.87
0.80	6693	1163	14.5	10.9	1493	35.7	89.3	15.7	1.79	14.8	2.18
0.75	8564	1476	17.2	13.8	1063	42.8	106	18.3	1.99	17.1	2.51
0.70	10664	1821	20.1	17.0	748	50.8	126	21.1	2.21	19.5	2.86
0.65	13036	2203	23.4	20.6	522	59.8	147	24.4	2.44	22.1	3.22
					1542/Average Granite						
0.95	6215	471	16.6	9.78	1508	44.4	117	19.3	1.92	13.5	1.77
0.90	9778	732	18.0	12.5	1102	49.5	129	21.2	2.07	15.0	1.96
0.85	13734	1017	19.4	15.5	796	55.2	144	23.3	2.24	16.5	2.16
0.80	18153	1330	21.0	18.8	357	61.7	160	25.7	2.41	18.1	2.37
					1542/73255c						
0.95	6415	522	16.7	8.06	1493	42.8	113	18.8	1.93	12.8	1.66
0.90	10199	838	18.0	8.90	1075	46.1	121	20.1	2.09	13.4	1.73
0.85	14400	1184	19.5	9.82	761	49.9	131	21.6	2.27	14.1	1.80
0.80	19093	1563	21.1	10.8	528	54.1	141	23.2	2.45	14.8	1.88
					1542/12033,517						
0.95	4433	473	17.7	9.66	1511	46.0	121	19.9	1.95	14.2	1.88
0.90	6029	737	20.3	12.2	1107	53.0	138	22.4	2.14	16.2	2.18
0.85	7800	1026	23.0	15.1	803	60.7	157	25.3	2.33	18.4	2.50
0.80	9779	1342	26.1	18.2	578	69.5	178	28.4	2.54	20.8	2.83
0.75	12006	1691	29.4	21.7	415	79.3	203	32.0	2.77	23.3	3.19

composition of VHK basalts. As a maximum of 8% granite assimilation (of either 73255c or average granite) is required, it appears that only K is radically affected (see Figs. 9-11).

The conclusion of *Neal et al.* (1988b) requiring at least two VHK basalt flows at the Apollo 14 site can be modified. Our modeling suggests that there must be at least three parental HA magmas required to generate the observed VHK basalt compositions. The range in VHK basalt textures and mineral compositions (*Neal et al.*, 1989) is consistent with the whole-rock chemistry. For example, VHK basalts containing no olivine have high abundances of incompatible elements (i.e., evolved mineralogies and whole-rock compositions). Conversely, VHK basalts, which are finer grained and contain high-Fo olivine phenocrysts, contain lower abundances of incompatible elements (i.e., are more primitive). The more evolved VHK basalts came from an evolved HA parental magma and vice versa. As demonstrated above, HA basalts form a continuum of compositions as a result of KREEP assimilation. We regard VHK basalts as offshoots from this HA basalt evolution trend by granite replacing KREEP as the assimilant. This adds support to a KREEP-granite relationship as suggested by *Ryder* (1976) and *Neal and Taylor* (1988). Once again, the importance of lunar granite cannot be overemphasized in light of the new VHK basalt clasts recovered from Apollo 14 breccias.

The recent work of *Dickinson et al.* (1988) has highlighted the importance of the siderophile element concentrations in Apollo 14 HA and VHK basalts. These authors noted that the Ge abundances in both HA and VHK basalts could not be generated using the proposed end members of our AFC model. Rather, Ge must have been enriched by several orders of magnitude over observed concentrations in 15386 KREEP and twice that in lunar granite. However, we do not feel that this negates the proposed AFC models for HA and VHK basalt petrogenesis. A pure KREEP composition has not as yet been defined. KREEP may be the magma composition either prior to silicate liquid immiscibility (SLI) or a mixture of the high-SiO_2 and high-Fe SLI melt products (*Neal and Taylor*, 1988, 1989). *Dickinson et al.* (1988) suggested that Ge partitions into the high-Fe melt during SLI. Therefore the Ge abundances in Apollo 14 HA and VHK basalts may be generated by the following scenario. The HA basalts are formed by assimilation of a KREEP component dominated by the high-Fe SLI melt product ("REEP-Frac"). This contains high abundances of REE (*Neal and Taylor*, 1989) and Ge (*Dickinson et al.*, 1988). This would also reduce the amount of crystallization and KREEP assimilation required by our present illustrative model in order to generate evolved HA basalts. Very high potassium basalts are produced by granite ("K-Frac"), replacing KREEP as the assimilant. As the VHK basalt compositions are basically controlled by the parental HA magma, high Ge abundances are inherited from the KREEP component, not granite. The work of *Dickinson et al.* (1988) emphasizes the need for further considerations of the composition of "pure" KREEP.

CONCLUSIONS

The analysis of new Apollo 14 basalt clasts has allowed the testing of previously formulated models for HA and VHK basalt petrogenesis (*Neal et al.*, 1988a,b). The results demonstrate the validity of these models, as the new major- and trace-element data can be accommodated, with only minor refinements. These refinements require that the parental HA basalt undergo 70% fractional crystallization (15.4% KREEP assimilation) in order to generate all HA basalt compositions at the Apollo 14 site. Furthermore, the new data emphasize the continuum of HA compositions. A review of Apollo 14 HA basalt isotope data is at present being undertaken in order to further test our AFC model. We predict that the more evolved HA basalts will exhibit slightly higher $^{87}Sr/^{86}Sr$ and slightly lower $^{143}Nd/^{144}Nd$ ratios than their more primitive counterparts. This reflects the higher Rb/Sr and lower Sm/Nd ratios in the KREEP assimilant.

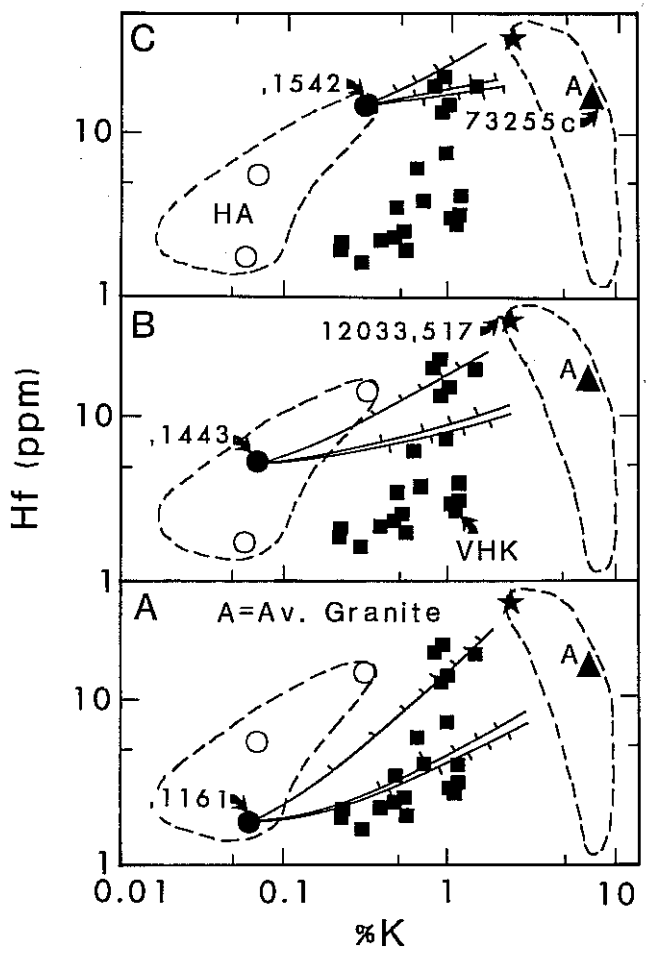

Fig. 11. Percent K vs. Hf (ppm) for HA and VHK basalts, and lunar granite. The AFC paths have been calculated (tick marks represent 5% increments of fractional crystallization—2.5% granite assimilation) between the parental HA basalts and granite assimilants 12033,517, average granite, and 73255c. A: HA basalt 14321,1161 is taken as parental; B: HA basalt 14321,1443 is taken as parental; C HA basalt 14321,1542 is taken as parental.

The modeling of VHK basalts by AFC has resulted in at least three VHK basalt flows being identified at the Apollo 14 site. These contain low, intermediate, and high abundances of incompatible elements, respectively. The use of granite 12033,517, in addition to 73255c and the average composition as assimilants, allows the variability of VHK basalt compositions to be accounted for. Both the major and trace-element concentrations of VHK basalts are controlled primarily by the parental magma, as the maximum amount of granite assimilation required to generate VHK compositions is only 8%. Only K appears to be radically affected. The high Ge abundances in Apollo 14 HA and VHK basalts may require a reevaluation of the KREEP assimilant used in our modeling. The results presented above demonstrate the intricate nature of basalt petrogenesis at the Apollo 14 site and emphasizes the likelihood of a granite-KREEP association within the lunar crust.

Acknowledgments. We wish to thank the Curatorial Staff in the Planetary Materials Branch at Johnson Space Center for their excellent assistance in processing the Apollo 14 breccia "pull-aparts" for us. The constructive discussions with A. Patchen and G. Ryder, J. Shervais, and J. Taylor are appreciated. Thoughtful reviews by C. Goodrich and an anonymous reviewer enhanced the quality of this manuscript. The research presented in this paper was supported by NASA funding to L.A.T. (grant no. NAG 9-62) and R.A.S. (grant no. NAG 9-63).

REFERENCES

Arth J. G. and Hanson G. N. (1975) Geochemistry and origin of the early Pre-Cambrian crust of north-eastern Minnesota. *Geochim. Cosmochim. Acta, 39,* 325-362.

Binder A. B. (1982) The Mare Basalt magma source region and Mare Basalt magma genesis. *Proc. Lunar Planet. Sci. Conf. 13th,* in *J. Geophys. Res., 87,* A37-A53.

Blanchard D. P. and Budahn J. R. (1979) Remnants from the ancient lunar crust: clasts from consortium breccia 73255. *Proc. Lunar Planet. Sci. Conf. 10th,* pp. 803-816.

Blanchard D. P., Jacobs J. W., and Brannon J. C. (1977) Chemistry of ANT-suite and felsite clasts from consortium breccia 73215 and of gabbroic anorthosite 79215. *Proc. Lunar Sci. Conf. 8th,* pp. 2507-2524.

DePaolo D. J. (1981) Trace element and isotopic effects of combined wallrock assimilation and fractional crystallization. *Earth Planet. Sci. Lett., 53,* 189-202.

Dickinson T., Taylor G. J., Keil K., Schmitt R. A., Hughes S. S., and Smith M. R. (1985) Apollo 14 aluminous mare basalts and their possible relationship to KREEP. *Proc. Lunar Planet. Sci. Conf. 15th,* in *J. Geophys. Res., 90,* C365-C374.

Dickinson T., Bild R. W., Taylor G. J., and Keil K. (1988) Late-stage enrichment of Ge in the magma ocean: evidence from lunar basalts (abstract). In *Lunar and Planetary Science XIX,* pp. 277-278. Lunar and Planetary Institute, Houston.

Dostal J., Dupuy C., Carron J. P., Guen L., and Maury R. C. (1983) Partition coefficients of trace elements: applications to volcanic rocks of St Vincent, West Indies. *Geochim. Cosmochim. Acta, 47,* 525-533.

Drake M. J. and Weill D. F. (1975) Partition of Sr, Ba, Ca, Y, Eu^{2+} and Eu^{3+}, and other REE between plagioclase feldspar and magmatic liquid: an experimental study. *Geochim. Cosmochim. Acta, 39,* 689-712.

Goodrich C. A., Taylor G. J., Keil K., Kallemeyn G. W., and Warren P. H. (1986) Alkali Norite, Troctolites, and VHK Mare Basalts from breccia 14304. *Proc. Lunar Planet. Sci. Conf. 16th,* in *J. Geophys. Res., 91,* D305-D318.

Haskin L. A. and Korotev R. L. (1977) Test of a model for trace element partition during closed-system solidification of a silicate liquid. *Geochim. Cosmochim. Acta, 41,* 921-939.

Hess P. C., Rutherford M. J., Guillemette R. N., Ryerson F. J., and Tuchfeld H. A. (1975) Residual products of fractional crystallization of lunar magmas: An experimental study. *Proc. Lunar Sci. Conf. 6th,* pp. 895-909.

Hughes S. S., Delano J. W., and Schmitt R. A. (1988) Apollo 15 yellow-brown glass: Chemistry and petrogenetic relations to green volcanic glass and olivine-normative mare basalts. *Geochim. Cosmochim. Acta,* in press.

Irving A. J. (1975) Chemical, mineralogical, and textural systematics of non-mare melt rocks: Implications for lunar impact and volcanic processes. *Proc. Lunar Sci. Conf. 6th,* pp. 363-394.

Irving A. J. and Frey F. A. (1984) Trace element abundances in megacrysts and their host basalts: Constraints on partition coefficients and megacryst genesis. *Geochim. Cosmochim. Acta, 48,* 1201-1221.

Lindstrom M. M., Marvin U. B., and Mittlefeldht D. W. (1989) Apollo 15 Mg- and Fe-norites: A redefinition of the Mg-suite differentiation trend. *Proc. Lunar Planet. Sci. Conf. 19th,* this volume.

Longhi J. (1977) Magma oceanography 2: Chemical evolution and crustal formation. *Proc. Lunar Sci. Conf. 8th,* pp. 601-621.

McKay G. A. and Weill D. F. (1976) Petrogenesis of KREEP. *Proc. Lunar Sci. Conf. 7th,* pp. 2427-2447.

McKay G. A., Wagstaff J., and Yang S. -R. (1986) Zr, Hf, and REE partition coefficients for ilmenite and other minerals in high-Ti lunar mare basalts: an experimental study. *Proc. Lunar Planet. Sci. Conf. 16th,* in *J. Geophys. Res., 91,* D229-D237.

Neal C. R. and Taylor L. A. (1988) "K-Frac + REEP-Frac": A new understanding of KREEP in terms of granite and phosphate petrogenesis (abstract). In *Lunar and Planetary Science XIX,* pp. 831-832. Lunar and Planetary Institute, Houston.

Neal C. R. and Taylor L. A. (1989) Metasomatic products of the lunar magma ocean: the role of KREEP dissemination. *Geochim. Cosmochim. Acta,* in press.

Neal C. R., Taylor L. A., and Patchen A. D. (1989) HA and VHK basalt clasts from Apollo 14 breccias: Part 1—Mineralogy and petrology. Evidence of crystallization from evolving magmas. *Proc. Lunar Planet. Sci. Conf. 19th,* this volume.

Neal C. R., Taylor L. A., and Lindstrom M. M. (1988a) Apollo 14 mare basalt petrogenesis: Assimilation of KREEP-like components by a fractionating magma. *Proc. Lunar Planet. Sci. Conf. 18th,* pp. 139-153.

Neal C. R., Taylor L. A., and Lindstrom M. M. (1988b) The importance of lunar granite and KREEP in Very High Poatassium (VHK) basalt petrogenesis. *Proc. Lunar Planet. Sci. Conf. 18th,* pp. 121-137.

Neal C. R., Taylor L. A., and Patchen A. D. (1988c) Basalts from Apollo 14 breccia 14321: Part 1—mineralogy and petrology (abstract). In *Lunar and Planetary Science XIX,* pp. 835-836. Lunar and Planetary Institute, Houston.

Neal C. R., Taylor L. A., Schmitt R. A., Hughes S. S., and Lindstrom M. M. (1988d) Basalts from Apollo 14 breccia 14321: Part 2—geochemistry (abstract). In *Lunar and Planetary Science XIX,* pp. 841-842. Lunar and Planetary Institute, Houston.

Neal C. R., Taylor L. A., Schmitt R. A., Hughes S. S., and Lindstrom M. M. (1988e) VHK basalt petrogenesis: Further evidence from breccias 14303 and 14304 (abstract). In *Lunar and Planetary Science XIX,* pp. 843-844. Lunar and Planetary Institute, Houston.

Quick J. E., Albee A. L., Ma M.-S., Murali A. V., and Schmitt R. A. (1977) Chemical compositions and possible immiscibility of two silicate melts in 12013. *Proc. Lunar Sci. Conf. 8th,* pp. 2153-2189.

Ryder G. (1976) Lunar sample 15405: Remnant of a KREEP-Granite differentiated pluton. *Earth Planet. Sci. Lett., 29,* 255-268.

Salpas P. A., Shervais J. W., Knapp S. A., and Taylor L. A. (1985) Petrogenesis of lunar granites: The result of apatite fractionation (abstract). In *Lunar and Planetary Science XVI,* pp. 726-727. Lunar and Planetary Institute, Houston.

Schnetzler C. C. and Philpotts J. A. (1970) Partition coefficients of REE between igneous matrix material and rock-forming mineral phenocrysts—II. *Geochim. Cosmochim. Acta, 34,* 331-340.

Shervais J. W., Taylor L. A., and Lindstrom M. M. (1985a) Apollo 14 mare basalts: Petrology and geochemistry of clasts from consortium breccia 14321. *Proc. Lunar Planet. Sci. Conf. 15th,* in *J. Geophys. Res., 90,* C375-C395.

Shervais J. W., Taylor L. A., Laul J. C., Shih C. -Y., and Nyquist L. E. (1985b) Very High Potassium (VHK) basalt: Complications in Mare Basalt petrogenesis. *Proc. Lunar Planet. Sci. Conf. 16th,* in *J. Geophys. Res., 90,* D3-D18.

Shih C.-Y. (1977) Origins of KREEP basalts. *Proc. Lunar Sci. Conf. 8th,* pp. 2375-2401.

Shih C.-Y., Nyquist L. E., Bogard D. D., Bansal B. M., Weismann H., Johnson P., Shervais J. W., and Taylor L. A. (1986) Geochronology and petrogenesis of Apollo 14 Very High Potassium mare basalts. *Proc. Lunar Planet. Sci. Conf. 16th,* in *J. Geophys. Res., 91,* D214-D228.

Vaniman D. T. and Papike J. J. (1980) Lunar highland melt rocks: Chemistry, petrology, and silicate mineralogy. *Proceedings of the Conference on the Lunar Highlands Crust* (J. J. Papike and R. B. Merrill, eds.), pp. 271-337. Pergamon, New York.

Villemant B., Jaffrezic H., Joron J. L., and Treuil M. (1981) Distribution coefficients of major and trace elements: fractional crystallization in the alkali basalt series of Chaine des Puys (Massif Central, France). *Geochim. Cosmochim. Acta, 45,* 1997-2016.

Walker D., Longhi J., and Hays J. R. (1972) Experimental petrology and origin of Fra Mauro rocks and soil. *Proc. Lunar Sci. Conf. 3rd,* pp. 797-817.

Walker D., Longhi J., Grove T. L., Stolper E., and Hays J. F. (1973) Experimental petrology and origin of rocks from the Descartes Highlands. *Proc. Lunar Sci. Conf. 4th,* pp. 1013-1032.

Warner R. D., Taylor G. J., Keil K., Ma M. -S., and Schmitt R. A. (1980) Aluminous mare basalts: New data from Apollo 14 coarse fines. *Proc. Lunar Planet. Sci. Conf. 11th,* pp. 87-104.

Warren P. H., Taylor G. J., Keil K., Shirley D. N., and Wasson J. T. (1983) Petrology and chemistry of two "large" granite clasts from the moon. *Earth Planet. Sci. Lett. 64,* 175-185.

Warren P. H., Shirley D. N., and Kallemeyn G. W. (1986) A potpourri of pristine moon rocks, including a VHK mare basalt and a unique, Augite-rich Apollo 17 anorthosite. *Proc. Lunar Planet. Sci. Conf. 16th,* in *J. Geophys. Res., 91,* D319-D330.

Warren P. H., Jerde E. A., and Kallemeyn G. W. (1987) Pristine moon rocks: A "large" felsite and a metal-rich ferroan anorthosite. *Proc. Lunar Planet. Sci. Conf. 17th,* in *J. Geophys. Res., 92,* E303-E313.